International Symposium
On Turbulence and Shear Flow
Phenomena (TSFP-9)
June 30 - July 3, 2015 *Melbourne, Australia*

SEMI-EMPIRICAL TURBULENCE MODELS SUITABLE FOR TRAILING EDGE NOISE PREDICTIONS

C. A. Albarracin
School of Mechanical Engineering
The University of Adelaide
South Australia 5005, Australia
cristobal.albarracingonzalez@adelaide.edu.au

C. J. Doolan
School of Mechanical and manufacturing Engineering
University of New South Wales
Sydney 2052, Australia
c.doolan@unsw.edu.au

ABSTRACT

An experimental investigation of the flow in the near wake of two struts with wedge-shaped trailing edges was conducted. The different trailing edge geometries give rise to three different boundary layers with different adverse pressure gradients. Measurements include mean and RMS velocity profiles, integral length scales, integral boundary layer properties and turbulent velocity spectra. Two autospectrum models were evaluated by comparing them to the experimental data, namely a Gaussian model and Pope's model spectrum. It was found that the Gaussian model agreed well with the data at low wave numbers, but decayed too rapidly for higher wave numbers, while Pope's spectrum overpredicted the amplitude at low wave numbers, but provided a good fit at high wave numbers. Based on the performance of these models, the Pope spectrum is more suitable for nose calculations

INTRODUCTION

Turbulent boundary layer flow over a sharp edged airfoil generates broadband noise, which can be detrimental in a variety of engineering applications, including aircraft, wind turbines and submarines. Understanding the flow over the trailing edge (TE) is paramount for the development of TE noise prediction methodologies, such as the RANS-based Statistical Noise Method (RSNM) (Albarracin *et al.*, 2012). This method requires a model of the turbulent velocity cross-spectrum near the TE, to link with the computed values of k and ε to calculate noise. The cross-specrum can be defined in terms of the auto-spectra at each point and the coherence function between the two points.

To the authors' best knowledge, there are no models of the turbulent velocity cross-spectrum for turbulent boundary layers subject to adverse pressure gradients (APG). This paper investigates the flow in the near wake of two flat struts with with wedged-shaped trailing edges. The different inclination angles of the trailing edges provide adverse pressure gradients of different strengths. The effect of the pressure gradient on the mean velocity profiles, RMS velocity profiles and length scales is investigated. The autospectrum of the streamwise velocity fluctuations is measured and two autospectrum models are evaluated, namely the auto-spectrum model of Pope (2000) and a Gaussian model,often used for noise modelling, based on the work of Morris & Farassat (2002).

EXPERIMENTAL SETUP

Experiments were performed in an open-jet low-speed wind tunnel at the University of Adelaide. The tunnel has a rectangular contraction outlet of dimensions 690 mm $\times$ 360 mm. The jet velocity was set at 6.4 m/s and the measured free stream turbulence intensity was $Ti = 0.65\%$. The models used in the experiment (Figure 1) are two 1.2 m chord struts of 25 mm thickness, with a wedge-shaped trailing edge with an apex angle of 12 degrees. Model 1 has a circular leading edge and model 2 has an elliptical leading edge. The trailing edge thickness is 1 mm. The boundary layer was tripped on both sides by a 0.5 mm thick turbulator strip placed at 10% chord. For the remainder of this paper, measurements on the bottom side (flat side) of model 2 will be referred to as the ZPG case, measurements on model 2 are referred to as APG 1 case, and measurements on the top side (inclined side) of model 2 are referred to as APG 2 case.

The models were positioned such that the leading edge coincided with the exit plane of the contraction outlet, and extension plates were fitted to the contraction outlet to ensure the trailing edge of the model was well within the potential core of the jet and measurements were not influenced by the nozzle lip shear layers. A depiction of the experimental setup is shown in Figure 2, with a coordinate system centered at the mid-span of the trailing edge and coinciding with the airfoil chord line. A pitot probe was positioned at $\mathbf{x} = (-1200, 84, 0)$ mm to monitor the free stream velocity.

A TSI 1210-T1.5 single wire probe with wire length of $L = 1.27$ mm and a wire diameter of $d = 3.81$ mm was

used, and it was operated using an IFA 100 constant temperature anemometer, with an overheat ratio of 1.8. The hot wire probe was mounted on a TSI 9400 2-axes traverse system, with a positional accuracy of 0.01 mm. The TSI traverse was controlled using the TSI-9400 traverse controller, which was connected to a computer via RS-232 port. Data were taken at 1 mm downstream of the trailing edge ($x = 1$ mm).

Data were acquired using a NI-PXI4472 data acquisition card, at a sample rate of 20 kHz for 8 seconds. A low-pass filter with a cut-off frequency of 8 kHz was applied to the data prior to digitization to avoid aliasing.

RESULTS

The boundary layer displacement thickness δ^* and momentum thickness θ were calculated from the mean velocity profiles according the the formulae

$$\delta^* = \int_0^\delta (1 - \frac{U}{U_\infty})dy \tag{1}$$

$$\theta = \int_0^\delta \frac{U}{U_\infty}(1 - \frac{U}{U_\infty})dy \tag{2}$$

where U_∞ is the free stream velocity and δ is the boundary layer thickness. The standard definition of δ as the location where the mean velocity reaches 99% of the free stream velocity is troublesome for flows with significant streamline curvature, such as flow over airfoils. In this work, δ is defined instead as the location where the gradient of the turbulence intensity reaches a small value.

$$\frac{dk}{dy} \leq 2 \times 10^{-5} \tag{3}$$

This value was chosen because it produces the same value of δ as using the 99% of the free stream velocity for the flat plate case. In order to accurately calculate the boundary layer thickness, a fifth degree polynomial was fitted to the data in the outer region of the boundary layer with a resolution of $dy = 0.01$ mm. Figure 3 shows the mean velocity profile and the curve fit used to calculate the boundary layer thickness for the ZPG case. The calculated boundary layer parameters are shown in Table 1.

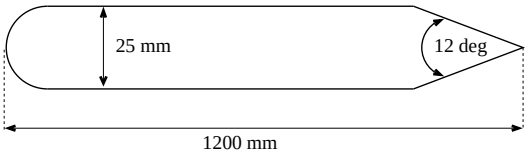

(a) Model 1.

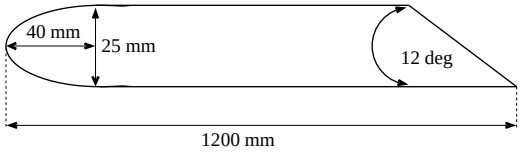

(b) Model 2.

Figure 1. Test cases used in the experiments. Model 1 has a circular leading edge. Both models have a trailing edge of 1 mm thickness.

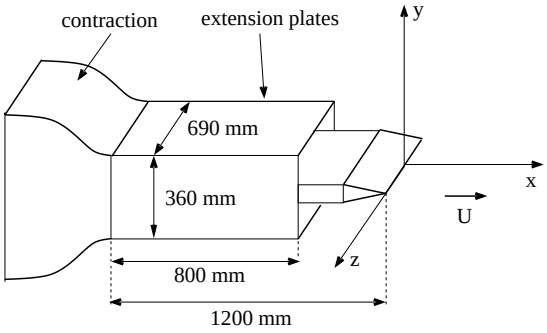

Figure 2. Schematic of the wind tunnel contraction with extension plates and model used in the experiments. The coordinate system was centered at the trailing edge of the model at the mid span point.

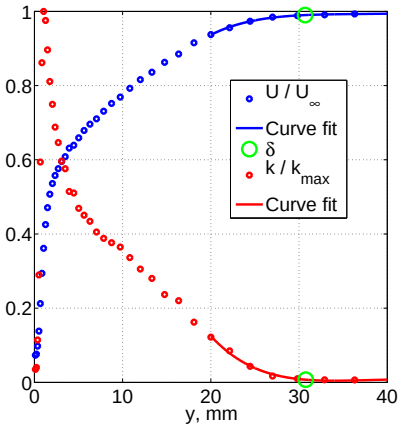

Figure 3. Mean Velocity and turbulent kinetic energy profiles and curve fits used to calculate the boundary layer thickness δ, measured 1 mm downstream of the trailing edge of the ZPG case.

The pressure gradient paramenter β is defined as

$$\beta = \frac{\delta^*}{\tau_w}\frac{dP}{dx} \tag{4}$$

where $\tau_w = \rho u_\tau^2$ is wall shear stress. The pressure gradient ($\frac{\partial p}{\partial x}$) was obtained from CFD simulations by taking the pressure over the surface of the airfoil between $0.95 \leq x/c \leq 1$ and calculating the slope by applying a linear fit to the data, as shown in Figure 4.

The friction velocity u_τ and the skin friction coefficient C_f were determined from the mean velocity profiles using the Clauser methodClauser (2003).

The combined effects of the APG and low Reynolds number of the current test cases make the logarithmic region of the boundary layer very small, making it difficult to

Table 1. Boundary layer parameters for all cases

case	δ/c	δ^*/δ	θ/δ	H	u_τ	β	R_θ	C_f
ZPG	0.026	0.181	0.117	1.55	0.3019	0.13	1.67×10^3	3.9×10^{-3}
APG 1	0.032	0.208	0.130	1.60	0.2513	0.83	2.21×10^3	2.7×10^{-3}
APG 2	0.024	0.237	0.139	1.70	0.2458	1.18	1.84×10^3	2.6×10^{-3}

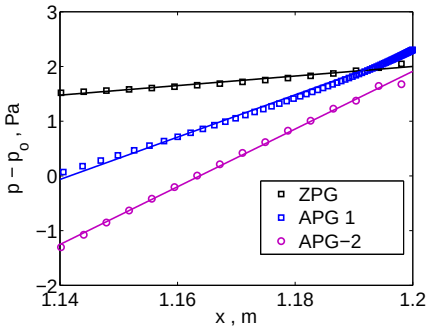

Figure 4. Pressure on the surface for all cases obtained from CFD. Solid lines are curve fits.

obtain the friction velocity using the Clauser method. Furthermore, it has been established that estimating u_τ with the Clauser method can result in significant errors in the presence of APG (Harun, 2012).

A shape factor of $1.3 \leq H \leq 1.5$ corresponds to turbulent flow, and a value of $H = 2.6$ indicates laminar flow. Therefore, the present results of 1.55 to 1.7 indicate that the flow is mostly turbulent and well developed.

The mean and RMS velocity profiles, normalized by viscous scales, are plotted in Figures 5(a) and 5(b), respectively, and compared to data from the literature. It can be observed that the data for the ZPG case follows the law of the wall very well between $30 < y^+ < 100$, and also compares well with the DNS data of Spalart (1988) for a turbulent boundary layer of similar Reynolds number. The extent of the log-region for the current data is much smaller than for the data of Klebanoff (1954). This is a consequence of the Reynolds number being lower for the present case ($Re_\delta = 13300$) than for Klebanoff's data ($Re_\delta = 152000$).

As Figure 5(b) shows,the RMS velocity profile for the ZPG case agrees reasonably well with the experimental data of Purtell *et al.* (1981) and with the DNS data of Spalart (1988), both corresponding to zero pressure gradient boundary layers of $Re_\theta = 1340$ and $Re_\theta = 1410$, respectively. The agreement deteriorates for the stronger APG cases. The adverse pressure gradient causes a secondary peak at $y^+ = 100$ in the RMS velocity profile for the stronger APG cases, its amplitude increasing with increased APG. This effect has also been observed by (Harun, 2012).

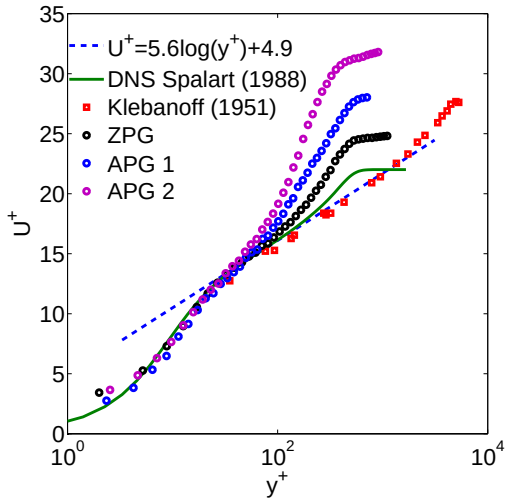

(a) Mean Velocity

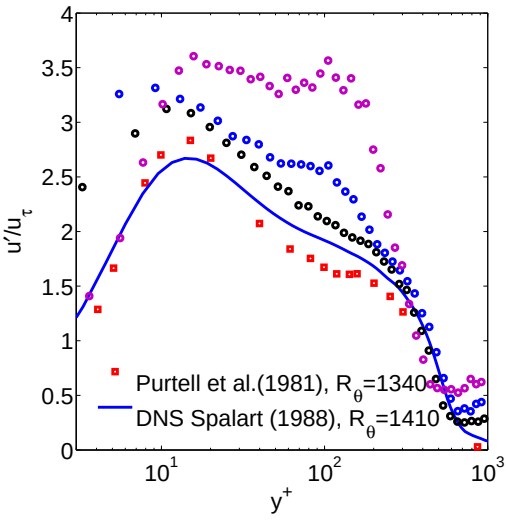

(b) RMS velocity

Figure 5. Mean and RMS velocity profiles in wall units. Measurements taken 1mm downstream of the TE. Circles in Figure 5(b) as in legend of Figure 5(a).

GAUSSIAN MODEL SPECTRUM

The first model is a Gaussian formulation based on the work of Morris & Farassat (2002).

$$E_{11}(\mathbf{y_1},\omega) = Au_s^2 \exp\left(-\frac{(U_c^2\kappa)^2}{4\omega_s^2}\right) \qquad (5)$$

where U_c is the convection velocity, and the velocity, frequency and time scales are defined as

$$u_s = \sqrt{2k/3},\ \ \omega_s = 2\pi/\tau_s,\ \ \tau_s = c_\tau k/\varepsilon \qquad (6)$$

k and ε can be determined from experimental data or from RANS CFD. In order to complete the model, the empirical

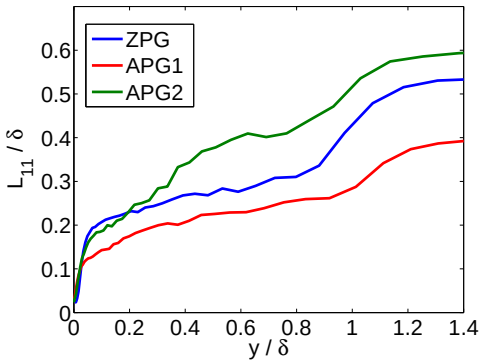

Figure 6. Longitudinal length scale normalized by boundary layer thickness. Data obtained at x=1 mm downstream of the trailing edge.

parameters A, c_ℓ and c_τ must be determined.

To isolate A, we can investigate the autospectrum at $\kappa = 0$,

$$E_{11}(\mathbf{y_1}, 0) = A u_s^2 \tag{7}$$

Solving for A and assuming isotropic turbulence, we obtain

$$A = \frac{3}{2k} E_{11}(\mathbf{y_1}, 0) = \frac{E_{11}(\mathbf{y_1}, 0)}{\langle u_1^2 \rangle} = \frac{2}{\pi} L_{11} \tag{8}$$

Therefore, A is proportional to the longitudinal length scale of the flow, L_{11}. This lengthscale can be determined from experimental data, or approximated by $L_{11} \approx k^{3/2}/\varepsilon$, which can be obtained from RANS CFD. L_{11} is shown in Figure 6 as a function of y/δ. It tends to zero as the wall is approached, and grows towards the edge of the boundary layer, where it reaches a value between $0.25\delta \leq L_{11} \leq 0.5\delta$, depending on the pressure gradient.

Having determined the value of A, the autospectrum is now

$$E_{11}(\mathbf{y_1}, \kappa) = \frac{2 L_{11} u_s^2}{\pi} \exp\left(-\frac{U_c^2 \kappa^2}{4\omega_s^2} \right) \tag{9}$$

To determine c_τ, we can integrate the autospectrum model to calculate $\langle u_1^2 \rangle$ and minimize the difference between the experimental and calculated value, or alternatively, the model autospectrum can be fitted to experimental autospectrum data using a least squares approach. Since $\langle u_1^2 \rangle$ can be obtained for RANS CFD, the former approach is preferred and used here. Figures 7(a) and 7(b) show the Gaussian autospectrum model compared to the experimental data in linear and logarithmic axes, respectively. The agreement is good at low wave numbers, however, for $\kappa \geq 100$, the model spectrum decays too fast.

POPE'S MODEL SPECTRUM

A model energy spectrum $E(\kappa)$ is proposed by Pope (2000) in the form

$$E(\kappa) = C_1 \varepsilon^{2/3} \kappa_1^{-5/3} f_L(\kappa_1 L) f_\eta(\kappa_1 \eta) \tag{10}$$

where $C_1 = 1.5$ and $L = k^{3/2}/\varepsilon$ is a length scale. The non-dimensional functions f_L and f_η determine the shape of the energy containing range and the dissipation range, respectively. The function f_L is given by

$$f_L(\kappa_1 L) = \left(\frac{\kappa_1 L}{[(\kappa_1 L)^2 + C_L]^{1/2}} \right)^{5/3 + p_0} \tag{11}$$

where p_0 is taken to be 2, and C_L is a positive constant. The function f_η is defined as

$$f_\eta(\kappa_1 \eta) = \exp\left(-\beta \left[(\kappa\eta)^4 + C_\eta^4 \right]^{(1/4)} - C_\eta \right) \tag{12}$$

to obtain the longitudinal spectrum we can integrate the energy spectrum using

$$E_{11}(\kappa_1) = \int_{\kappa_1}^{\infty} \frac{E(\kappa)}{\kappa} \left(1 - \frac{\kappa_1^2}{\kappa^2} \right) d\kappa \tag{13}$$

The coefficients C_L and C_η are $C_\eta \approx 0.4$ and $C_L \approx 6.78$ for high Reynolds number. Alternatively, they can be determined from the one-dimensional spectrum by enforcing

$$\int_0^{\infty} E_{11}(\kappa_1) d\kappa_1 = \langle u_1^2 \rangle \tag{14}$$

In this work, $C_\eta = 0.4$ was used, and C_L was obtained from equation 14.

Pope's model spectrum is shown in Figures 7(a) and 7(b) at selected locations in the boundary layer for the APG1 case and compared to the Gaussian model and experimental data. The model overpredicts the spectra at $\kappa \leq 80$, but it follows the experimental data well for high wave numbers.

CONCLUSIONS

An experimental investigation of the flow in the near wake of two struts with wedge-shaped trailing edges was conducted. The different trailing edge geometries give rise to three different boundary layers with different pressure adverse gradients. It was observed that increasing the pressure gradient makes the logarithmic region of the boundary layer smaller, and causes the velocity profile to depart from the log law with an increased slope. The adverse pressure gradient also causes an increase in the shape factor H. Increasing the pressure gradient also gives rise to a secondary peak in the turbulent kinetic energy at $y^+ \approx 100$, which increases in amplitude as the APG increases. The velocity autospectrum was measured and two autospectrum models were evaluated by comparing them to the experimental data, namely a Gaussian model and Pope's model spectrum. It was found that the Gaussian model agreed well with the data at low κ, but decayed too rapidly for higher wave numbers. Pope's spectrum overpredicted the amplitude at low wave numbers, but provided a good fit at high κ.

REFERENCES

Albarracin, CA, Doolan, CJ, Jones, RF, Hansen, CH, Brooks, LA & Teubner, MD 2012 A rans-based statistical noise model for trailing edge noise. In *Proceeding*

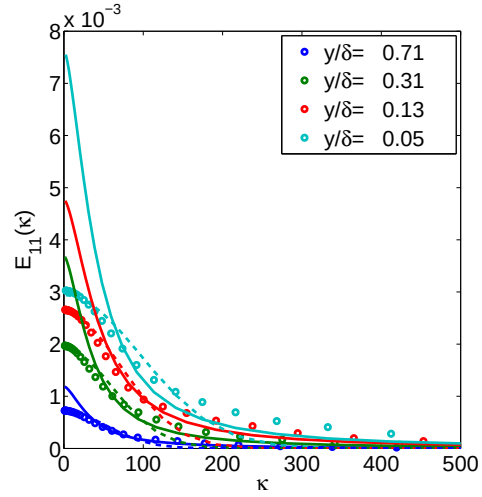

(a)

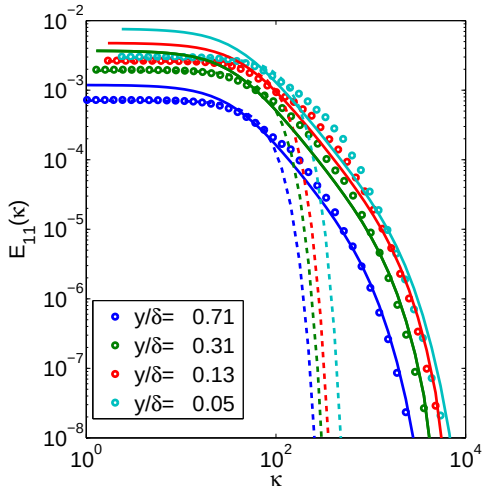

(b)

Figure 7. Longitudinal autospectrum as a function of wave number at selected points in the boundary layer for the APG1 case. Symbols: experimental data, dashed lines: Gaussian model, solid lines: Pope's Model.

of the 18th AIAA/CEAS Aeroacoustics Conference, AIAA Paper, , vol. 2181.

Clauser, F.H. 2003 Turbulent boundary layers in adverse pressure gradients. *AIAA JOURNAL* **41** (7; SUPP/A), 238–255.

Harun, Zambri 2012 The structure of adverse and favourable pressure gradient turbulent boundary layers. PhD thesis, Department of Mechanical Engineering, University of Melbourne.

Klebanoff, PS 1954 Characteristics of turbulence in a boundary layer with zero pressure gradient. naca report 1247, nasa–langley research center, hampton, va, 1955. *Tech. Rep.*. See also NACA Technical Note 3178.

Morris, P. J. & Farassat, F. 2002 Acoustic analogy and alternative theories for jet noise prediction. *AIAA Journal* **40** (4), 671–680.

Pope, Stephen B 2000 *Turbulent flows*. Cambridge university press.

Purtell, Lawrence Patrick, Klebanoff, PS & Buckley, FT 1981 Turbulent boundary layer at low reynolds number. *Physics of Fluids* **24**, 802.

Spalart, Philippe R 1988 Direct simulation of a turbulent boundary layer up to rj= 1410. *Journal of Fluid Mechanics* **187** (1), 61–98.